JGR Biogeosciences

RESEARCH ARTICLE
10.1029/2025JG008759

Microbial Resuscitation and Growth Rates in Deep Permafrost: Lipid Stable Isotope Probing Results From the Permafrost Research Tunnel in Fox, Alaska

T. A. Caro[1], J. M. McFarlin[2], A. E. Maloney[1], S. D. Jech[3], A. J. Barker[4], T. A. Douglas[4], R. A. Barbato[4], and S. H. Kopf[1]

[1]Department of Geological Sciences, University of Colorado Boulder, Boulder, CO, USA, [2]Department of Geology and Geophysics, University of Wyoming, Laramie, WY, USA, [3]Department of Ecology and Evolutionary Biology, University of Colorado Boulder, Boulder, CO, USA, [4]US Army Cold Regions Research and Engineering Laboratory, Ft. Wainwright, AK, USA

Key Points:

- Microbial growth is extremely slow within the first 30 days of thaw. Temperature may drive which taxa are active, but not growth rates
- Subsurface microbes preferentially produce glycolipids over phospholipids, suggesting a role in cryotolerance
- Ancient, entrapped gases may be the primary source of emissions in early thaw stages

Supporting Information:

Supporting Information may be found in the online version of this article.

Correspondence to:

T. A. Caro,
Tristan.Caro@colorado.edu

Citation:

Caro, T. A., McFarlin, J. M., Maloney, A. E., Jech, S. D., Barker, A. J., Douglas, T. A., et al. (2025). Microbial resuscitation and growth rates in deep permafrost: Lipid stable isotope probing results from the permafrost research tunnel in Fox, Alaska. *Journal of Geophysical Research: Biogeosciences*, *130*, e2025JG008759. https://doi.org/10.1029/2025JG008759

Received 9 JAN 2025
Accepted 11 SEP 2025

Author Contributions:

Conceptualization: T. A. Caro, J. M. McFarlin, R. A. Barbato, S. H. Kopf
Data curation: T. A. Caro
Formal analysis: T. A. Caro, A. E. Maloney, S. D. Jech, S. H. Kopf
Funding acquisition: S. H. Kopf
Investigation: T. A. Caro, J. M. McFarlin, A. E. Maloney
Methodology: T. A. Caro, J. M. McFarlin, A. E. Maloney, S. H. Kopf
Project administration: S. H. Kopf
Resources: T. A. Caro, J. M. McFarlin, A. J. Barker, T. A. Douglas, R. A. Barbato, S. H. Kopf
Software: T. A. Caro, S. D. Jech, S. H. Kopf
Supervision: S. H. Kopf
Validation: T. A. Caro
Visualization: T. A. Caro
Writing – original draft: T. A. Caro

Abstract Permafrost is at increasing risk of thaw as cold regions in the Northern Hemisphere continue to warm. The lability of organic carbon in permafrost post-taw largely depends on the rate at which microorganisms resuscitate and proliferate after many years in freezing, dark, anaerobic conditions. Moreover, the bulk of the Earth's permafrost exists at deep subsurface horizons, far below the active layer, that have been isolated for hundreds, thousands, or millions of years. However, the resuscitation and growth rates of microorganisms in deep permafrost remain unknown. To quantify these rates, we conducted lipid stable isotope probing (lipid-SIP) on permafrost cores of late-pleistocene age from four locations within the Permafrost Research Tunnel near Fairbanks, Alaska. We compare rates of microbial growth, marker gene sequences, and greenhouse gas (CO_2, CH_4) emissions across cores held anaerobically at ambient (−4°C) and elevated temperatures (4°C, 12°C). In deep, ancient permafrost, microbial growth is exceedingly slow, often undetectable, within the first month following thaw, indicating a notable lag period, where only 0.001%–0.01% of cells turn over per day. This suggests a "slow reawakening" that could provide some buffer between anomalous warmth and C degradation if permafrost refreezes seasonally but remains anaerobic. However, within 6 months, microbial communities undergo dramatic restructuring and become distinct from both the ancient and overlying surface communities. These results have critical implications for predictions of microbial biogeochemical contributions in a warming arctic, especially as thaw proceeds into deeper and more ancient permafrost horizons.

Plain Language Summary Permafrost, frozen earth material containing soil, rock, and ice, harbors more organic carbon than is currently in the atmosphere as CO_2. As the Arctic warms and permafrost thaws, ancient microbes can reactivate, allowing the degradation of organic carbon that has accumulated in permafrost over millenia, resulting in the release of greenhouse gases. In this work, we measured the rates at which permafrost microorganisms resuscitate during thaw and related these growth rates to changes in microbial community composition and greenhouse gas emissions. We find that microbes in thawing subsurface permafrost exhibit a slow "reawakening" at first, but within 6 months the microbial community undergoes dramatic changes. Microbial communities that survive and proliferate after burial for thousands of years do not resemble those on the surface and exhibit reduced diversity. Finally, we note that microbes in subsurface permafrost rely on different kinds of lipids to construct their cell membranes: these compounds may have helped them survive freezing, dark conditions for millenia.

1. Introduction

Permafrost, typically defined as soil, rock, and ice that has been frozen for at least two consecutive years, comprises roughly one quarter of land area in the Earth's Northern Hemisphere and stores a massive quantity of Earth's carbon, estimated to be twice as large as the amount of CO_2 currently in the atmosphere (Hugelius et al., 2014). The Arctic is warming at approximately two to four times the global rate (Rantanen et al., 2022; Stocker, 2014). Microbial degradation processes enabled by thaw threaten to release permafrost stores of organic carbon as CO_2 or CH_4. In Alaska, the majority of permafrost exists to depths exceeding 10 m (Jorgenson et al., 2008) and underlies over 80% of Alaska's surface area. Near Fairbanks, discontinuous permafrost reaches depths of up to 97 m (Jorgenson et al., 2008). In continuous permafrost regions on Alaska's north slope,

Writing – review & editing: T. A. Caro, J. M. McFarlin, A. E. Maloney, A. J. Barker, T. A. Douglas, R. A. Barbato, S. H. Kopf

permafrost depth has been measured in excess of 660 m (Jorgenson et al., 2008). Therefore, a massive fraction of permafrost volume exists in deep subsurface horizons that are inaccessible to surface operations and difficult or impossible to assess with remote sensing. As temperature and anthropogenic landscape disturbances increase across the Arctic, permafrost thaw will presumably proceed further into deep subsurface horizons. Therefore, studies investigating the response of subsurface permafrost are urgently needed to understand its response to warming Arctic conditions.

Within permafrost lies a biosphere in suspended animation. A fraction of microorganisms emplaced in permafrost at time of deposition (freezing) survive and persist at sub-zero temperatures through low-energy maintenance and repair (Price & Sowers, 2004). While buried and frozen, permafrost-hosted microorganisms may exhibit low levels of metabolic activity, likely as a result of trace liquid water available as brines within interstitial spaces even at sub-freezing temperatures (Bakermans et al., 2003; Gilichinsky et al., 1993; Nikrad et al., 2016; Rivkina et al., 2000). Thaw remobilizes liquid water, a previously limited resource, thereby liberating both microorganisms and any attendant organic matter. Numerous studies have examined the identity and genomic characteristics of microorganisms in permafrost (Mackelprang et al., 2017), as well as how these communities shift during thaw (Barbato et al., 2022; Burkert et al., 2019; Romanowicz & Kling, 2022; Waldrop et al., 2023), proposing mechanisms for how these communities experience ecological succession as a result of initial deposition (properties of the paleoenvironment), environmental filtering i.e., selection), and thaw characteristics (Doherty et al., 2020; Ernakovich et al., 2022; Waldrop et al., 2023). During thaw, microbial communities reassemble after extreme environmental selection imposed by energy limitation and dark, freezing conditions. This thaw period is marked by microbial resuscitation, activity, and finally, proliferation.

Despite numerous studies investigating microbial identity, diversity, and functional capacity in permafrost, the growth rates of microorganisms under both ambient and thaw conditions are unknown. Anabolic activity, expressed as biomass production, is a critical parameter to assess ecosystem functioning, habitability, and ecological dynamics (Foley et al., 2024). Measurements of microbial anabolic activity can provide estimates for resuscitation time—the lag before microbial growth resumes (Aanderud et al., 2015). Additionally, growth is a mediator of microbial community assembly: knowing how quickly microorganisms are growing informs theories of microbial community succession (Ernakovich et al., 2022; Foley et al., 2024; Weissman et al., 2021). Measurements of microbial growth rates, in both frozen and thawed conditions, are essential for a predictive understanding of microbial contributions to permafrost degradation and greenhouse gas emissions.

To conduct this study, we applied lipid stable isotope probing (lipid-SIP) on samples collected from the Permafrost Tunnel operated by the U.S. Army Cold Regions Research and Engineering Laboratory (CRREL). The Tunnel, located in Fox, AK (64.951256°N, 147.620731°W) is an ideal study site because it provides access to deep permafrost horizons, ranging in age from the modern to the late Pleistocene (>40 kya), allowing study across permafrost of varying age (Barbato et al., 2022; Burkert et al., 2019; Douglas et al., 2011; Leewis et al., 2020; Mackelprang et al., 2017; Waldrop et al., 2023) (Figure 1). Lipid-SIP has been demonstrated to be a sensitive measure of microbial growth in a variety of settings including soil (Caro et al., 2023), clinical settings (Kopf et al., 2016), and marine sediments (Wegener et al., 2012). Lipid-SIP is a favorable technique for measuring the exceedingly low rates of growth expected in permafrost because of the sensitivity of the GC-P-IRMS technique applied, which is capable of measuring biomass generation times that far exceed the incubation duration. With lipid-SIP, we target phospholipid fatty acids (PLFAs), as PLFAs are an optimal analyte to assess microbial community size due to the fact that they rapidly degrade upon cell death and therefore provide quantitative estimates of standing and produced microbial biomass (Frostegård et al., 2011; Zhang et al., 2019). We additionally include analysis of glycolipids as glycolipid fatty acids (GLFAs). Glycolipids are of interest as they may replace phospholipids in the membrane during periods of nutrient deprivation via replacement of the phosphate headgroup with a carbohydrate (Jones et al., 2021; Peng et al., 2019; Stankeviciute et al., 2019). Glycolipids are also hypothesized to play role in cryoprotection by sequestering divalent cations, resulting in the production of a saline gel around the cell (Casillo et al., 2019; Corsaro et al., 2017).

To date, the resuscitation and biomass production rates of microorganisms hosted in subsurface permafrost have never been measured. To address this key knowledge gap, we pursued a study of near-surface and subsurface permafrost with three objectives: (a) measure the biomass production of microorganisms at both ambient and thaw conditions, (b) compare anabolic rates to 16S rRNA amplicon surveys to investigate the connection between

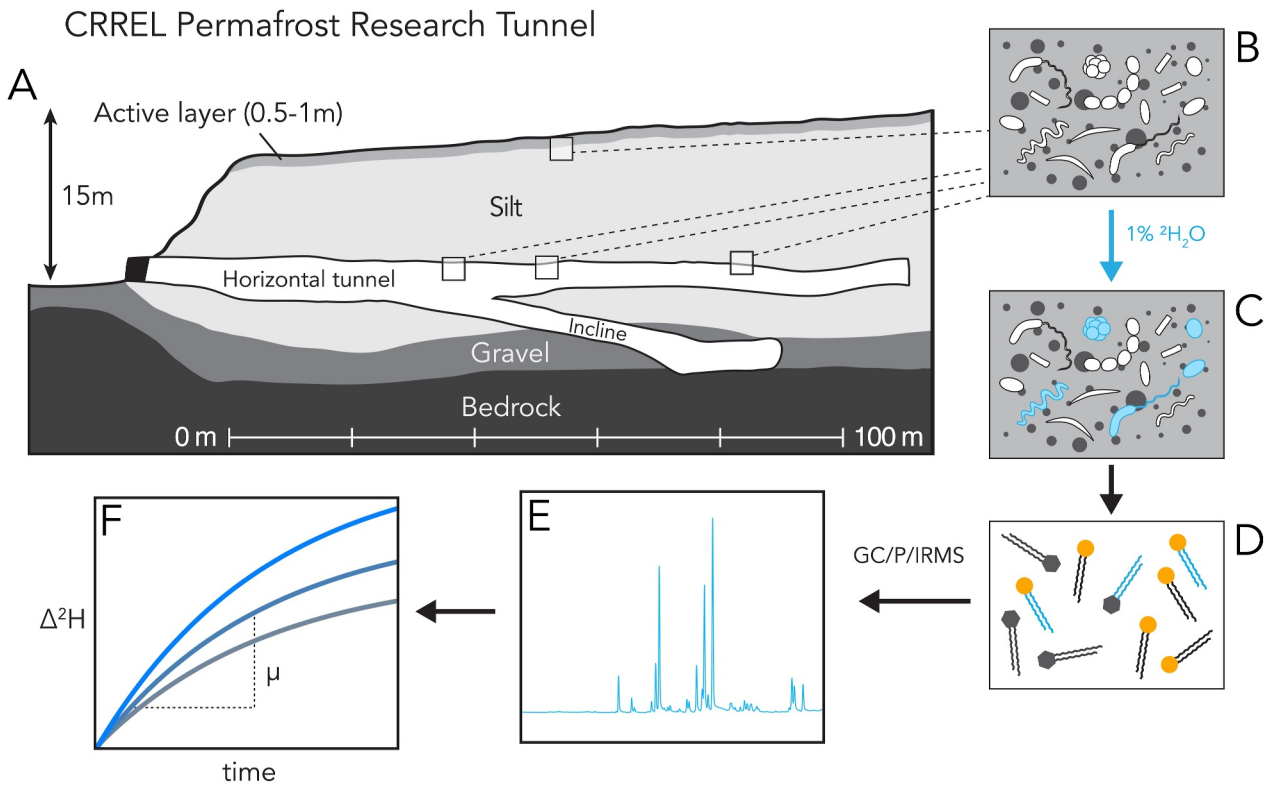

Figure 1. Schematic overview of study site and experimental procedure. (a) Cross section of the northern corridor of the CRREL Permafrost Tunnel in Fox, AK. The tunnel provides access to subsurface permafrost dated to the late Pleistocene. (b) Samples of permafrost from both near-surface and subsurface intervals contain relict microorganisms emplaced during initial permafrost development. (c) Lipid biosynthesis is a key expression of anabolic activity, and its detection represents microbial resuscitation and growth following thaw. Resuscitated microorganisms in the presence of deuterated "heavy" water tracer (1 at. % ^2H) incorporate ^2H into newly produced lipids. (d) Intact polar lipids are extracted from permafrost incubations. Lipids are separated into phospholipid (circle) and glycolipid (hexagon) fractions by headgroup polarity. (e) The deuterium composition of fatty acid chains are analyzed by GC/P/IRMS. (f) The rate of deuterium enrichment (Δ^2H) of individual lipids, relative to their isotopic composition at the beginning of the experiment, is used to calculate the growth rate (μ) of individual lipid compounds or the aggregate microbial community.

microbial growth and community succession, (c) evaluate the link between anabolic rates and the emission of greenhouse gases (CO_2 and CH_4).

2. Materials and Methods

2.1. Permafrost Sampling and SIP Incubation

Permafrost was collected from the U.S. Army Cold Regions Research and Engineering Laboratory Permafrost Tunnel located in Fox, Alaska, on 6 August 2021 (Figure 1). Cores of 1 m in length were recovered using a gas-powered SIPRE (Snow, Ice, and Permafrost Research Establishment) corer (Jon's Machine Shop, Fairbanks, Alaska, USA). Above the permafrost tunnel, the peat and thawed soil layers (where "active layer" refers to perennially thawed soil layers) were first removed with an ethanol-sterilized knife and trowel to access the frozen permafrost layer. The SIPRE corer was subsequently mounted to the frozen permafrost layer and a vertical core was extracted. Cores extracted from within the tunnel itself were drilled horizontally into the pore-ice cemented silt of the tunnel wall at distances of 35, 54, and 83 m from the tunnel portal (Figure 1a). After recovery, all cores were enclosed in PVC tubing and stored inside the tunnel, which is held at −3°C.

All personnel wore Tyvek suits, personal N95 respirators, and nitrile gloves during core collection to reduce potential contamination. The SIPRE cores and all tools were cleaned with 70% isopropyl alcohol. Cores were stored in insulated boxes containing ice packs (Thermosafe U-Tek) to maintain temperature for shipping. All samples were transported to the Institute for Arctic and Alpine Research (INSTAAR) at the University of

Colorado Boulder and stored at −20°C until processing. Temperature loggers (iButton) were included in each shipment to confirm the internal temperature of the shipments never exceeded 0°C during transport.

In the laboratory, permafrost cores were sectioned using a diamond-blade table-top tile saw. The saw was operated in a lab at room temperature (~20°C). Samples were rapidly transferred from and returned to a −20°C freezer. Before each sample, the saw blade and surface were cleaned with ultrapure water and 70% isopropyl alcohol. Then, the saw blade and metal saw table surface were cleaned by sequential triple rinsing with methanol (MeOH), dichloromethane (DCM), and hexane in a fume hood to remove organic contaminants. The saw was kept clean of dust and debris between samples by covering its work surface with combusted aluminum foil. To process the cores for incubation, a cylindrical subsection of the intact core was cut, its exterior pared away, wrapped in combusted aluminum foil, and stored at −20°C until incubation. When beginning the incubation, the core subsection was unwrapped and cut into 12 subsections, one for each incubation time point and temperature condition. For each incubation, a subsection of core (approx. 70—100 g wet weight) was weighed and added to a 250 mL bottle along with 50 mL of filter-sterilized anaerobic $^{2}H_2O$ (1 at. % ^{2}H) and the bottle was sealed with a butyl stopper. Incubation headspace was flushed with N_2 for 30 min before being placed in a temperature-controlled incubator held at either −4°C, 4°C, or 12°C. Near-surface permafrost samples were only incubated at 12°C. Samples were incubated for either 0, 7, 30, or 180 days. At the end of the experimental period, microbial growth was arrested by transferring incubations to a −70°C freezer.

At the end of the SIP incubation period, and before freezing, permafrost was transferred to 50 mL centrifuge tubes and excess water was separated from permafrost pellets by centrifugation. Excess incubation water was filtered through a 0.2 μm syringe filter before storage. Isotopic composition of the incubation water was measured to account for the isotopic contributions of water native to the permafrost and in order to quantify the effective strength of the SIP tracer. Both permafrost and excess water were frozen at −70°C. Frozen permafrost pellets were lyophilized for 48 hr and stored at −70°C until lipid extraction.

2.2. Headspace Gas Measurements

Incubation headspace CO_2 and CH_4 were measured on a Silco SRI 8610C Gas Chromatograph Flame Ionization Detector (GC-FID) equipped with a methanizer. 0.5 mL of gas was anaerobically sampled from the incubations and injected using a gas-tight syringe. The GC-FID was equipped with a 2 m, 2 mm ID, ShinCarbonST 80/100 column and held at 200°C for each run. Gas concentrations were determined by comparison to a standard mix of 1% CO, CO_2, CH_4, which was periodically injected to account for instrument drift.

2.3. Lipid Extraction

Intact polar lipids were extracted from the lyophilized permafrost pellets using a modified Bligh and Dyer lipid extraction (Bligh & Dyer, 1959; Quideau et al., 2016). In brief, 5.0 g of freeze-dried soil was added to a solvent-cleaned PTFE centrifuge tube. 50 μg of 23:0 phosphatidylcholine (23:0-PC) internal standard was added to each tube prior to extraction. Three extraction mixes of different polarities, Solutions A, B, and C were applied. Solution A consisted of 1:2:0.8 (v:v:v) dichloromethane (DCM), methanol (MeOH), and phosphate buffer (8.7 g/L K2HPO4, 3.5 mL/L 6N HCl). Solution B consisted of 1:2:0.8 (v:v:v) DCM, MeOH, and trichloroacetic acid (TCA) buffer (250 mL 10% TCA, 250 mL H2O, 8.8 g KOH). Solution C is a 1:5 (v:v) mixture of DCM and MeOH, respectively. 20 mL of each extraction solution was applied to the lyophilized pellet in sequence. To extract organics, the mixture was vortexed for 20 s, sonicated in an ultrasonic bath for 10 min, then centrifuged at 3,000 G for 10 min. After centrifugation, the supernatant was carefully pipetted and added to a collection vial. The sample was extracted with Solution A twice, Solution B twice, and Solution C once. To separate organic and aqueous components, phase separation was induced by the addition of 25 mL ultrapure water followed by 25 mL DCM. Phases were allowed to separate for at least 2 hr, then the organic (bottom) phase was removed by pipetting. All samples were dried in a TurboVap LV at 35°C under a stream of N_2 and stored at −20°C prior to downstream steps. With each batch of samples extracted, a contamination blank was processed simultaneously. No contamination was observed in process blanks. All glassware was combusted at 450°C for 8 hr prior to use. All PTFE vials were triple solvent rinsed with MeOH, DCM, and Hexane prior to use.

2.4. Intact Polar Lipid Separation and Derivatization

First, to remove residual extraction water and polar impurities, total lipid extract (TLE) was run through a sodium sulfate sand column (500 mg 80:20 w/w Na_2SO_4:silica sand). The cleaned TLE eluent was then collected and purified using silica gel chromatography (Quideau et al., 2016) to focus isotopic analyses on intact polar lipids derived from intact cells. Combusted silica solid-phase extraction (SPE) columns containing 500 mg SiO_2 were conditioned with the addition of 5 mL acetone, then two additions of 5 mL dichloromethane (DCM). TLE was redissolved in 0.5 mL DCM and transferred to the SPE column. Neutral lipids were eluted with the addition of 5 mL of DCM. Glycolipids were eluted by the addition of 5 mL acetone. Phospholipids were eluted by the addition of 5 mL MeOH. Each fraction was collected separately in combusted vials.

The glyco- and phospholipid extracts were derivatized to fatty acid methyl esters (FAMEs) via base-catalyzed transesterification using methanolic base (Griffiths et al., 2010; Rodríguez-Ruiz et al., 1998). Transesterification was initiated by adding 2 mL hexane and 1 mL 0.5 M NaOH in anhydrous methanol to dry lipid extracts. The reaction mixture proceeded for 10 min at room temperature before being quenched by the addition of 140 μL of glacial acetic acid and 1 mL water. The organic phase was extracted three times with 4 mL hexane and dried under a stream of N_2. A recovery standard of 10 μg 21-phosphatidylcholine (21:0 PC) was added to each lipid fraction before derivatization to assess reaction yield.

2.5. FAME Quantification and Identification

A Thermo Trace 1310 Gas-Chromatograph equipped with a DB5-HT column (30 m × 0.250 mm, 0.25 μm) coupled to a flame ionization detector (GC-FID) was used to quantify FAME concentrations based on peak area relative to the 23:0-PC extraction standard and a palmitic isobutyl ester (PAIBE) quantification standard, respectively. FAMEs were suspended in 100 μL n-hexane and 1 μL was injected using a split-splitless injector (SSL) run in splitless mode at 325°C; column flow was constant at 1.2 mL/min. The GC ramped according to the following program: 80°C for 2 min, ramp at 20°C/min for 5 min (to 140°C), ramp at 5°C/min for 35 min (to 290°C). The FID was held at 350°C for the duration of the run. Major peaks were identified by retention time relative to a Bacterial Acid Methyl Ester (BAME) standard (Millipore-Sigma) and a 37 FAME standard (Supelco). Due to the uncertainty associated with identifying double bond position and stereochemistry for FAMEs containing multiple double bonds, unsaturated and poly-unsaturated compounds are identified only tentatively based on the position and retention time relative to the above standards. FAMEs are referred to using the nomenclature z-x:y, where x is the total number of carbons in the fatty acid skeleton and y is the number of double bonds and their position (if known), while z-is a prefix describing additional structural features of the compound such as branching, methylation, and cyclization. FAMEs were quantified using an external standard curve of PAIBE (Figure S1 in Supporting Information S1).

2.6. FAME Hydrogen Isotope Analysis

The hydrogen isotopic composition of FAMEs was quantified on a Thermo Scientific 253 Plus stable isotope ratio mass spectrometer coupled to a Trace 1310 GC via Isolink II pyrolysis/combustion interface (GC/P/IRMS). Chromatographic conditions were as such: 40°C for 2 min, 20°C/min to 180°C, 5°C/min to 265°C, 30°C/min to 330°C, hold for 1.84 min, He carrier flow rate was 1.2ccm, the programmable temperature vapourization inlet temperature was ramped from 40°C to 400°C. Peaks were identified based on retention order and relative height based on coregistration with GC-FID chromatograms. Peak areas and isotopic values for mono- and di-unsaturated FAMEs were integrated to reduce uncertainty in downstream calculations at the expense of reduced compound specificity (e.g., all 16:1 isomers are reported simply as "16:1"). Measured isotope ratios were corrected for scale compression, linearity, and memory effects using standards of both natural abundance and isotopically enriched fatty acid esters of known isotopic compositions ranging from −231.2 ‰ to +3,972 ‰ versus Vienna Standard Mean Ocean Water (VSMOW). Memory (peak-to-peak carryover) was corrected for using our previously defined framework (Caro et al., 2023). Hydrogen isotope calibrations were performed in R using the packages *isoreader* (v.1.4.1) and *isoprocessor* (v.0.6.11) (Kopf et al., 2021). Calibrated isotope ratios were corrected for the H added during derivatization to FAMEs: the hydrogen isotope composition of methanol used for base-catalyzed transesterification was measured by derivatizing with phthalic acid with a known H isotopic composition (Arndt Schimmelmann, Indiana University) via acid catalysis. The resulting phthalic acid methyl ester (PAME) was analyzed by GC/P/IRMS and this correction was applied to all measured FAMEs.

2.7. Growth Calculations

Calculation of biomass synthesis based on FAME enrichment is possible because the hydrocarbon chains of intact polar lipids consist only of C-H bonds that are nonexchangeable on biological timescales, unlike the readily exchangeable H bound to O, N, and S in lipid headgroups, proteins, and nucleic acids. The ^{2}H tracer is therefore stably incorporated into newly synthesized fatty acid tails during anabolic activity. Biomass synthesis rates are calculated as described previously (Caro et al., 2023; Kopf et al., 2016). In brief, lipid biosynthesis *(r)* reflects a combination of growth (μ) and repair (ω), where *r, μ, and ω* refer to specific biosynthesis rates (day^{-1}) and $r = \mu + \omega$. Our measurements therefore provide an upper bound for the specific growth rate (μ) and lower bound for the apparent generation time (T_G) of a given lipid (and its microbial source):

$$r = -\frac{1}{t} \cdot \ln \frac{F_t - a \cdot F_L}{F_0 - a \cdot F_L} \tag{1}$$

$$\mu \leq r \tag{2}$$

$$T_G = \frac{\ln(2)}{\mu} \geq \frac{\ln(2)}{r} \tag{3}$$

These calculations yield compound-specific growth rate and generation time estimates that can be viewed by themselves or aggregated into assemblage-level estimates of community growth by calculating an abundance-weighted mean:

$$\text{weighted mean} = \frac{\sum_{i=1}^{N} x_i w_i}{\sum_{i=1}^{N} w_i} \tag{4}$$

where x_i is the isotopic fractional abundance of compound i and w_i is the relative abundance (weighting) of compound *i.* As discussed, these estimates aggregate cell-to-cell variations in growth. Uncertainty in each set of measurements was propagated through our calculations of μ by standard error propagation (Caro et al., 2023). We note that the "biomass generation times" reported in this work may be distinct from microbial "doubling times" because our method is unable to ascribe quantified biosynthesis to cell fission events. The generation times we report represent the time for biomass doubling assuming constant biosynthesis. Indeed, cell growth in oligotrophic environments may never lead to cell division, but rather the replacement of existing biomass. We therefore call the metric here an "apparent" growth rate/generation time, as it represents a maximum growth rate assuming no biosynthesis of lipids occurs for maintenance or other non-growth activities.

To assess microbial biomass production at extremely low rates, we took steps to increase our confidence in measurements of enriched ^{2}H both at the compound-specific and assemblage (abundance weighted mean) levels. First, isotopically-enriched samples were followed by aggressive cleaning blanks where the instrument was ramped and held at a high (350°C) isothermal temperature followed by flushes of H_2 reference gas. Second, isotopic compositions of individual FAMEs were corrected for memory effects as described in (Caro et al., 2023), which reduces the possibility that ^{2}H enrichment observed is the result of previous chromatographic peaks contaminating the peak of interest. Third, we define conservative thresholds for detection of deuterium enrichment and quantification of biomass production. We define our ^2F detection limit as:

$$\text{Detected:} \quad {}^2F_T - \sigma_{FT} > {}^2F_0 + \sigma_{F0}$$

$$\text{Not detected:} \quad {}^2F_T - \sigma_{FT} \leq {}^2F_0 + \sigma_{F0}$$

where ^2F_T is isotopic fractional abundance of a sample/compound at time of sampling (T), $^2F_0$ is the isotopic fractional abundance of a sample/compound at the start of the experiment ($T = 0$), and σ represents associated calibration error. For calculations of growth (μ), we apply standard error propagation. This propagated error results in an uncertainty term for biomass production rate (σ_μ). We separately designate our limit of growth rate quantification as:

$$\text{Quantifiable:} \quad \sigma_\mu/\mu < 1$$

$$\text{Not quantifiable:} \quad \sigma_\mu/\mu \geq 1$$

where the fraction σ_μ/μ represents the relative error in the rate measurement. In other words, propagated error in growth rate must be less than the growth rate value itself to meet our criteria for quantification.

The terms "relative" and "absolute" growth rate are used according to (Foley et al., 2024) where relative growth rate is the change in biomass or population relative to starting size (e.g., day^{-1}) and absolute growth rate is the rate of change in mass per unit time (e.g., pg day^{-1}). Relative growth rate measurements were converted to absolute growth rates by:

$$\mu_{abs} = \mu_{rel} \times m \tag{5}$$

where μ_{abs} is the absolute growth rate in units of mass per time per mass of permafrost [pg $(day \cdot g)^{-1}$ permafrost], μ_{rel} is growth rate in units of inverse time (day^{-1}), and m is the permafrost weight-normalized lipid mass (pg lipid/g permafrost) measured by GC-FID and calculated based on the extraction and derivatization efficiency determined by internal standards (Materials and Methods Section 2.4). Cell abundances were estimated by multiplying PLFA and GLFA abundances by the mean conversion factor (3.5×10^{-3} pg PLFA/cell) estimated by Frostegård and Bååth (1996). Resuscitated fraction (RF), the fraction of cells that resuscitate in a period of time, is defined as:

$$RF_T = \frac{m_{produced}}{m_{total}} \times T \approx \frac{n_{produced}}{n_{total}} \times T \tag{6}$$

where $m_{produced}$ is the mass of produced biomass within the time period of interest (T), m_{total} is the total biomass of the sample; $n_{produced}$ and n_{total} are estimates of cell abundances converted from biomass. In this work, we report the fraction resuscitated after one day [$RF_{(1\ day)}$].

2.8. 16S Ribosomal RNA Gene Sequencing

DNA was extracted from permafrost subsamples in triplicate and with negative controls (empty vials) using the DNEasy PowerSoil Pro DNA Isolation Kit (Qiagen) according to the manufacturer's instructions with the following modifications: three triplicate extractions (via bead beating) were pooled onto a single elution column in order to increase the concentration of recovered DNA. DNA was cleaned (PCR inhibitors removed) with a DNEasy PowerClean Kit (Qiagen) with no modifications to the manufacturer's protocol.

Extracted DNA samples were amplified in duplicate using Platinum II Hot-Start PCR Master Mix (ThermoFisher Scientific) SimpliAmp thermocyclers (ThermoFisher). The 16S rRNA gene primers 515F and 806R (V4 amplification) with Illumina sequencing adapters and unique 12-bp barcodes were used as described by the Earth Microbiome Project (Apprill et al., 2015; Parada et al., 2016). The PCR program was 94°C for 2 min followed by 35 cycles of 94°C (15 s), 60°C (15 s), 68°C (1 min), and a final extension at 72°C for 10 min. Amplification was evaluated by agarose gel electrophoresis. Amplicons were cleaned and normalized with the SequalPrep Normalization Plate (Thermo Fisher Scientific) following the manufacturer's instructions and then pooled together. Pooled libraries were quantified using both the Qubit ds DNA High Sensitivity Assay (ThermoFisher) and the KAPA Library Quantification Kit for Illumina platform (Roche). Sequencing was performed on an Illumina MiSeq using a v2 500 cycle PE reagent kit with paired-end reads at the Center for Microbial Exploration, University of Colorado Boulder.

To prepare samples for analysis with the DADA2 bioinformatic pipeline (Callahan et al., 2016), reads were demultiplexed with adapters and primers were removed using standard settings for cutadapt. We used standard filtering parameters with slight modifications for 2×150 bp chemistry where forward reads were not trimmed, and reverse reads were trimmed to 140 base pairs. A maximum error rate (maxEE) of 2 was allowed. Taxonomy was assigned with the SILVA (v138) reference database (Quast et al., 2013). Data was analyzed and visualized using the phyloseq and MicroViz packages in R (Barnett et al., 2021; McMurdie & Holmes, 2013).

Table 1
Summary of Site Characteristics

	Surface	35 m	54 m	83 m
Description	Near-surface, 10 cm below active layer	Subsurface, 35 m from portal	Subsurface, 54 m from portal	Subsurface, 83 m from portal
Fraction modern	0.5936 ± 0.0014	0.0089 ± 0.0022	0.0057 ± 0.0022	0.0051 ± 0.0022
^{14}C Age (kya)	4.19 ± 0.02	37.9 ± 2	41.5 ± 3	42.4 ± 3.4
pH	6.45	7.1	6.39	6.51
EC (mmho/cm)	0.07	0.55	0.29	0.39
OM (%)	3.06	1.64	2.04	1.35
NO_3^- (ppm)	0.5	BDL	BDL	BDL
Total P (ppm)	30.4	57.8	75.4	35.8
Total S (ppm)	9.7	36.3	50.9	52.5
Total K (ppm)	339	174	168	199
Total C (%)	1.69	3.1	4.24	2.12
Total N (%)	0.08	0.17	0.30	0.22
Total IC	BDL	BDL	BDL	BDL
C:N Ratio	21	14	14	12

Note. "BDL" indicates below detection limit.

2.9. Water Stable Hydrogen Isotope Analysis

The labeled incubation waters, following 0.22 μm filtration through a PES membrane, were analyzed for the H stabe isotope composition (^2F_L) after gravimetric dilution with water of known isotopic composition (1:1000 w/w) to get into the analytical range of available in-house standards previously calibrated to VSMOW and Standard Light Antarctic Precipitation (SLAP). 1 μL of each sample was measured on a dual inlet Thermo Delta Plus XL isotope ratio mass spectrometer connected to an H-Device for water reduction by chromium powder at 850°C (Putman et al., 2017). Measured isotope values in δ notation on the VSMOW-SLAP scale were converted to fractional abundances using the isotopic composition of VSMOW ($R_{VSMOW} = {}^2H/{}^1H = 0.00015576$) (Meija et al., 2016) and corrected for the isotope dilution by mass-balance. The isotopic composition of each incubation was measured individually and resulted in values ranging between +30,065—49,153 ‰ versus VSMOW (0.481—0.775 at. % ^{2}H) These values were considered to be what cells encountered during tracer incubation (a combination of both the tracer and water present in the soil) and were applied to all growth rate calculations as ^2F_L.

2.10. Permafrost Dating and Characterization

Approximately 5 g of lyophilized subsample of each permafrost core (prior to incubation with stable isotope probes) was sent for radiocarbon age dating at the National Ocean Sciences Accelerator Mass Spectrometry (NOSAMS) facility at Woods Hole Oceanographic Institution (Woods Hole, MA, USA), which uses NBS Oxalic Acid I (NIST-SRM-4990) as a reference standard. Collected data corresponds to NOSAMS accession numbers OS-175451, OS-175452, OS-175453, OS-175454. Routine geochemical description of the permafrost was conducted at the Colorado State University Soil, Water, and Plant testing facility (Denver, CO, USA). In brief, a KCl extract was used to quantify soil nitrate. An AB-DTPA extract was used to quantify P and S. Organic matter was determined by mass loss on ignition.

3. Results and Discussion

3.1. Experiment Summary and Site Characteristics

In Table 1 we report key characteristics of the permafrost cores. Subsurface permafrost samples are of late Pleistocene age (37.9—42.4 kya). These samples exhibit lower C:N ratios than the near-surface core (4.19 kya), which could suggest organic matter (OM; i.e., lignin) degradation and nitrogen accumulation during burial (Mu et al., 2015).

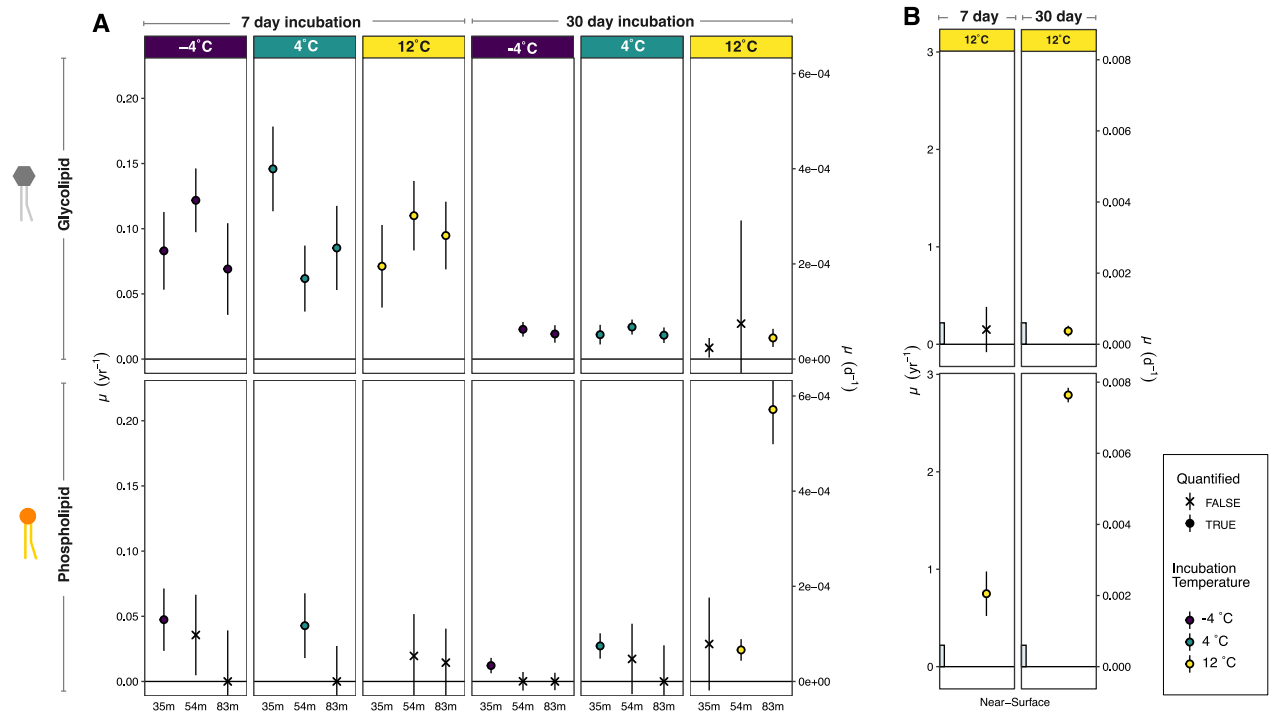

Figure 2. Microbial biomass growth in subsurface permafrost. The left axis indicates apparent growth rate (μ) in units of (yr^{-1}); the right axis notes μ in units of (d^{-1}). Data symbols represent whether growth could be reliably quantified; point color corresponds to thaw temperature. Error bars represent total propagated error including instrument error, calibration error, and growth calculations. Missing data points indicate PLFAs/GLFAs were not detected. (a) displays subsurface biomass growth rates. (b) displays near-surface growth rates. Note differences in *y* axes between panels (a, b). The *y*-axis limits of panel (a) are noted as a small blue rectangle in panel (b), for scale comparison. Data corresponding to the glycolipid and phospholipid fractions are plotted in the upper and lower panels, respectively. Each data point represents the weighted mean growth rate of all compounds detected in a given sample, normalized to the mass of permafrost in the incubation.

While previous work has identified a "chronosequence" along the tunnel wall, the ^{14}C dates measured here indicate that the subsurface samples may overlap chronologically (Barbato et al., 2022; Burkert et al., 2019; Leewis et al., 2020). While the 35, 54, and 83 m samples exhibit a positive trend with age, the higher error associated with carbon dating at these ages makes these values difficult to distinguish with confidence.

3.2. Microbial Resuscitation and Growth Differ Between Near-Surface and Subsurface Permafrost

In near-surface permafrost, microbial anabolic activity resumed following thaw. In brief, microbial growth is quantified as a function of the difference of ^{2}H abundance between microbial biomass at the start and end of an incubation (where biomass at the initial time is roughly natural abundance ^{2}H) (See: *Materials and Methods)*. ^{2}H enrichment proceeds more rapidly among PLFAs compared to GLFAs in near-surface permafrost (in contrast with subsurface samples: see Section 3.4). Robust microbial growth can be observed in as soon as 7 days in both phospho- and glycolipid lipid pools, with PLFAs exhibiting greater rates of production (Figure 2). ^{2}H enrichments in PLFA pools correspond to abundance-weighted average growth rates between 2.1×10^{-3} (d^{-1}) after 7 days and 7.6×10^{-3} (d^{-1}) after 30 days. The increase in growth rate observed (decrease in generation time) between the 7- and 30-day SIP incubations indicates that microbial growth rate itself is increasing with time (Figure 2). Growth rates correspond to community-level biomass generation times of 338 days (7 days incubation) and 91 days (30 days incubation). These rates are substantially slower than those previously inferred in soil. The most comparable estimates are previous measurements by Caro et al., who measured aggregate microbial generation times in high alpine tundra of 14–45 days during a 7-day incubation) (Caro et al., 2023).

With reliable estimates of lipid biomass or cell abundances, we convert measurements of relative growth rate (fractional replacement per unit time, e.g., day^{-1}) into absolute measurements of growth rate (in units of biomass (g) produced per unit time). Because intact polar lipids are quantitative indicators of intact microbial biomass in the environment, we calculate absolute growth rate by multiplying the PLFA or GLFA mass by production rate (Foley et al., 2024; Frostegård & Bååth, 1996). Measured PLFA content in near-surface permafrost varied

between 3.8–7.1 × 10^3 ng/g (Table S3 in Supporting Information S1). Measurements of absolute growth rate in near-surface permafrost therefore range between 1.4–54 ng PLFA/day/g. Similarly, GLFA content in near-surface permafrost varied between 3.8–6.0 × 10^6 pg GLFA/day/g, resulting in GLFA production rates of 1.4–2.5 ng GLFA/day/g.

In subsurface permafrost, microbial resuscitation and growth are much slower than near-surface samples and some are undetectable in the timescale of our 7 and 30 days incubations. For PLFAs, substantial ^{2}H enrichment was detected in only a fraction of subsurface samples (Table S2 in Supporting Information S1). When detected, inferred relative growth rates lie between 3.3 × 10^{-5} to 5.7 × 10^{-4} (d^{-1}), which correspond to community-level generation times of 3.3–57.5 years. PLFA abundances in subsurface core samples was substantially lower than near-surface samples, between 330 and 1,500 ng PLFA/g permafrost. Absolute rates of PLFA production in the subsurface therefore vary between 0 (undetectable) and 427 pg PLFA/day/g. Intriguingly, in subsurface samples, glycolipids exhibited more robust rates of production than phospholipids 4.4 × 10^{-5} to 4.0 × 10^{-4} (d^{-1}) (absolute growth rate: 68—624 pg/day/g permafrost), with all but 2 samples meeting detection criteria (Figure 2, Table S1 in Supporting Information S1) (Section 3.4). No clear relationship between microbial growth, incubation temperature, and incubation duration is observed in subsurface permafrost (Figure 2). In other words, some samples incubated at 12°C had lower rates of microbial growth than those incubated at 4°C and −4°C. Similarly, there was no clear trend between permafrost age and microbial growth rate (Figure 2).

We emphasize that our reported values of microbial growth rates are upper estimates. The relative contributions of maintenance and repair versus growth-related biosynthesis are unknown in natural environments. It is possible that the anabolic activity we detect is not in preparation for cell fission events but rather turnover of existing biomass. Additionally, microbial mortality among non-growing populations may also result in an over-estimation of growth rate. Therefore, actual rates of growth may be even slower than quantified.

3.3. Quantifying the Balance of Dormancy and Resuscitation

Intact polar lipids provide quantitative estimates of living microbial biomass and cell numbers due to their rapid decay following cell death and demonstrated relationships between lipid content and cell concentrations in soil (Frostegård & Bååth, 1996; Zhang et al., 2019). Measurements of microbial growth via lipid-SIP can therefore be tied directly to absolute estimates of anabolic activity across the microbial community, where the number of active cells out of the intact cell community can be estimated. e.g., in the near-surface permafrost core, we convert PLFA content to estimates of intact cell abundance and estimate cell densities of 1.7–2.0 × 10^9 cells/g permafrost. With lipid-SIP, we can therefore estimate that 4.0 × 10^5–1.6 × 10^7 cells are turned over daily over the course of 30 days.

If one assumes that microbial resuscitation is a discrete phenomenon (i.e., that measured isotopic growth is *only* the result of resuscitated cells), and that resuscitated cells contribute evenly to measured isotopic enrichment, then observed rates of biomass production can be a useful but imperfect metric of resuscitation rate. To this end, we calculate the resuscitated fraction (RF) of the microbial community with Equation 6 as the fraction of the microbiome that is resuscitated per day ($RF_{(1\ day)}$). In near-surface permafrost, the $RF_{(1\ day)}$ lies between 0.02% and 0.8% of cells resuscitated per day. Resuscitation fractions in subsurface samples are substantially lower, ranging between $RF_{(1\ day)}$ = 0.0044%–0.04% as estimated by GLFA synthesis and 0.0033%–0.057% by PLFA synthesis. Exceptionally low RFs are evidence of high heterogeneity in resuscitation processes, suggesting that an equivalent of only 1 in 10,000–100,000 intact cells are successfully resuscitated per day in subsurface permafrost. The caveat with these estimates is that, when growth rates are aggregated into community-level (abundance-weighted) means, lipid-SIP cannot describe intracommunity heterogeneity that is, the difference between one cell out of 100,000 undergoing complete turnover from 100,000 cells undergoing 10^{-5} turnover. However, we consider the calculation of RFs to be a useful and intuitive metric with which to frame microbial resuscitation and growth in this system. Indeed, in the anaerobic permafrost environment, high degrees of heterogeneity in resuscitation and growth is to be expected for dormant cells and spores, which use dormancy and non-uniform spontaneous resuscitation as a bet hedging strategy (Epstein, 2009; Lennon & Jones, 2011) and high resuscitation heterogeneity seems particularly likely given the observed trends in community composition (Section 3.5, Figure 3).

The interpretation of the RF changes if microbial activity in subsurface permafrost is not primarily a result of resuscitation, but microorganisms being constitutively active in frozen conditions. In this end-member scenario,

Figure 3. Microbial abundance across all samples and incubations. The horizontal axis of the main panel represents the fractional relative abundance of taxa grouped at the genus level (or highest annotated taxonomic rank, indicated in the key). The right-side panel indicates the Simpson alpha diversity index for each sample across incubations. Incubation time is noted on the *y*-axis; incubation temperature is noted in the right-hand panel labels.

the observed anabolic activity represents trace anabolic activity of cells already active within habitable permafrost microenvironments. Interpreting the RF in this context would indicate that minute traces of microbial biomass, ranging between 0.0044%–0.04% of GLFAs and 0.0033%–0.057% of PLFAs are turned over in active microbial populations, per day.

While lipid-SIP yields coarse taxonomic resolution, which is, at best, able to differentiate different phyla or broad functional groups (Caro et al., 2023; Willers et al., 2015a, 2015b), aggregating analytes from the entire microbial assemblage affords lipid-SIP the precision required to detect trace quantities of growth and estimate RFs. In contrast, single cell SIP analyses, such as those conducted with nanoscale secondary ion mass spectrometry (nanoSIMS) or Raman microspectroscopy (Caro et al., 2024; Eichorst et al., 2015), may not be suitable for permafrost environments due to the potentially miniscule fraction of the microbial community that is resuscitated in the early stages of thaw and the sensitivity required for single-cell measurement (Kopf et al., 2015).

A caveat of our methodology is the potential for persistence of PLFAs/GLFAs following cell death, which could lead to depressed estimates of microbial growth. We target our study toward fatty acids derived from intact polar lipids due to their rapid degradation upon cell death (Frostegård et al., 2011; Lipp et al., 2008; Schubotz et al., 2009; Zhang et al., 2019). However, free IPLs themselves could conceivably decay more slowly in low-temperature incubations due to hindered kinetics of IPL hydrolysis. By incubating over longer durations (up to 6 months), our goal was to minimize this risk, as phospholipid headgroup cleavage is thought to occur on the order of hours (Zhang et al., 2019).

3.4. Permafrost Exhibits Distinct Patterns of Microbial Glycolipid and Phospholipid Production

There exists an intriguing distinction between production rates of PLFAs and GLFAs in the near-surface and subsurface permafrost. Compared to PLFAs, GLFAs are an order of magnitude more abundant across the subsurface samples (Figure 2, Tables S1–S3 in Supporting Information S1) and produced at greater rates. In

subsurface permafrost, GLFA production was detected in 88% of incubations, whereas PLFA production was detected in 38% of incubations (Table S2 in Supporting Information S1). At the near-surface, the opposite trend is observed: GLFA production rates are far slower than their PLFA counterparts (Figure 2), despite similar PLFA and GLFA concentrations (PLFA: 5–7 × 10^6; GLFA: 4–6 × 10^6, Tables S1–S2 in Supporting Information S1). We suggest that the abundance of glycolipids, and their more robust production in subsurface environments, points to the preference of cold-adapted bacteria to produce glycolipids as an adaptation to long-term freezing conditions. Indeed, glycolipids have been identified as membrane components of a variety of psychrophilic bacteria and are important constituents of lipopolysaccharide layers (LPS), which itself functions as a cryoprotectant (Casillo et al., 2019; Corsaro et al., 2017). It has been speculated that the high negative charge density of core LPS may be related to the sequestration of divalent cations, which may provide anti-freezing benefits by promoting the presence of liquid water at the ice-brine-cell interface (Corsaro et al., 2017; Gilichinsky et al., 1993). Within the lipid membrane, glycolipids are known to replace phospholipids during nutrient (phosphorous) deprivation, as a carbohydrate can replace the more typical phosphate within the lipid head group (Jones et al., 2021; Peng et al., 2019; Stankeviciute et al., 2019). While we cannot unambiguously assign observed GLFAs to LPS structures or as standalone cell membrane constituents, their robust production in comparison to phospholipids in subsurface cores supports the idea that glycolipids may serve a long-term cryoprotective role for organisms buried in permafrost.

3.5. In the Long Term, Microbial Communities Undergo Substantial Restructuring After Thaw

As described, exceptionally slow rates of microbial growth are observed after 7 and 30 days incubation post-thaw (Tables S1 and S2 in Supporting Information S1). SIP incubations of 180 days experienced dramatic changes in microbial community structure, lipid content, and lipid production. Lipids analyzed from the 180 days subsurface incubations were extremely enriched in ^{2}H, up to 0.568 at.% (approx. δ^2H_{VSMOW} = +35,696 ‰). This observation is supported by striking increases in microbial biomass with time, across all incubation and temperature conditions (Figures S2–S7 in Supporting Information S1). Such isotopic enrichments approach that of the tracer solution, suggesting that prolific microbial growth has occurred, to the point where the bulk of the microbial constituency has undergone several doublings. The exact number of doublings cannot be estimated because isotope enrichment can no longer be quantitatively distinguished as cell biomass approaches isotopic parity with the tracer.

For the 35 and 83 m cores, the alpha diversity (Simpson) index decreases over the duration of thaw due to the proliferation of specific taxa (Figure 3). In the 35 m core, *Cryobacterium* and *Psychrobacillus* dominate at 4°C and *Desulfosporosinus, Planococcaceaea,* and *Pseudoarthrobacter* dominate at 12°C. Similarly, dominance of *Cryobacterium*, *Desulfosporosinus, and Pseudoarthrobacter* genera*; as well as Planococcaceaea* family, is observed after 180 days in the 83 m core. The 54 m core offers a striking contrast to the 35 and 83 m cores (Figure 3). This permafrost starts with an extremely homogenous microbial community dominated by *Clostridium sensu stricto 13*, a genus housing a variety of spore-forming species including *Clostridium bowmanii, Clostridium botulinum,* and *Clostridium huakuii. Clostridia* are more generally anaerobic spore-forming bacteria capable of fermenting soil organic matter (Boutard et al., 2014; Chades et al., 2018; Guan & Goldfine, 2021). Due to the dominance of a single taxa at the beginning of the incubation, the alpha diversity index (Simpson) increases over the course of thaw, as rare taxa begin to proliferate and balance the microbial community. After 180 days, the communities in core 54 m see a substantial reduction in the original *Clostridium sensu stricto 13* community, with new abundance of *Cryobacterium* and *Desulfosporosinus.* Dominant taxa in these samples such as *Desulfosporosinus*, a genus of sulfate reducing bacteria, *Clostridium sensu stricto 13*, and *Psychrobacillus*, are widely described as spore forming (Buehler et al., 2018; Hippe & Stackebrandt, 2015; Krishnamurthi et al., 2010; Spring et al., 2003). The 16S data coupled with previously discussed resuscitation rates points to the relevance of heterogeneous resuscitation (and the utility of RFs, as described above) because only a handful of community members, as low as 1–7 taxa, can emerge as dominant members of the microbial community.

The archaea detected in this study exhibit variation between cores and near-surface/subsurface (Figure S8 in Supporting Information S1), but these communities do not exhibit clear successional trends with time. Archaea within the permafrost samples of this study comprise, at most, 4% of the microbial community and more typically ∼1% (Figure S8 in Supporting Information S1). It is difficult to describe microbial succession of low-abundance microbial community members, as trace differences in abundance may be overprinted by the shifts of more abundant taxa. The 35 m subsurface core is dominated by ammonium oxidizing archaea (AOA) *Candidatus*

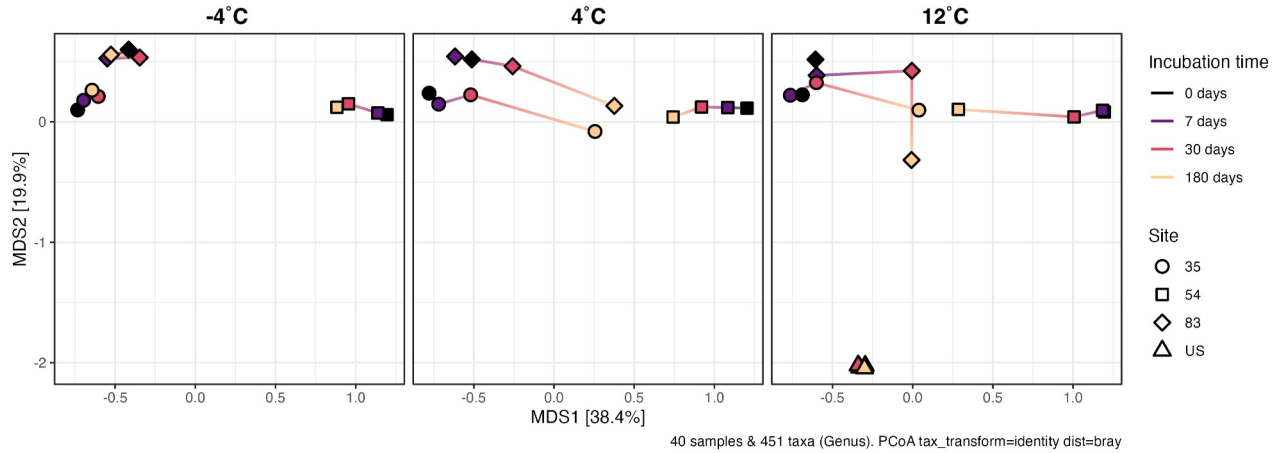

Figure 4. Microbial community similarity across incubation time series. Points are plotted based on Bray-Curtis dissimilarity. Point shape is the sampling site, where 35, 54, and 83 are distance from portal entrance in meters and "US" indicates Undisturbed near-Surface permafrost.

Nitrocosmicus Genus and Family *Nitrosphaeraceae.* Methanogenic archaea of genus *Methanobacterium* are the most abundant archaea in the 54 m subsurface core as well as the near-surface core. The 83 m core has low relative abundances of archaea but includes *Candidatus Nitrocosmicus* as well as Class *Bathyarchaeaia. Bathyarchaeaia* are notable as a diverse taxonomic group often associated with organic rich ecosystems and have been found capable of fermentation and acetogenesis of complex organic matter (Evans et al., 2015; He et al., 2016; Lazar et al., 2016).

Subsurface microbial communities become more similar over the course of thaw (Figure 4). However, these communities do not converge toward a composition resembling that of younger permafrost, but rather, they form a "revenant" microbial community that is clearly distinct from modern near-surface permafrost-hosted microbial communities (Figure 4). It is also important to note that the near-surface-hosted permafrost community maintained its structure over the course of thaw at 12°C and did not display indications of significant succession. These results suggest that near-surface permafrost sites may be poor proxies for predicting microbial community dynamics and responses in deeper horizons, which make up the bulk share of permafrost by volume (Jorgenson et al., 2008). The revenant community that we describe is the result of millennia of environmental filtering which includes the ancient depositional environment, duration of burial, metabolite, and energy limitation, etc (Ernakovich et al., 2022; Waldrop et al., 2023). The convergence of subsurface microbial communities toward a shared revenant community suggests that common selection forces may be shaping the trajectory of communities during thaw. Further investigation of microbial succession dynamics in permafrost is required for a predictive understanding of community responses to thaw and the identification of taxonomic "indicators" of thaw processes (Ernakovich et al., 2022).

Our lipid-SIP results indicate that rates of subsurface microbial resuscitation and anabolic activity do not relate to thaw temperature at temperatures above freezing. It is also clear from our 16S results that subsurface microbial communities held at above-freezing temperatures under anaerobic conditions undergo dramatic community turnover and succession after 180 days, whereas those held below freezing do not (Figure 3). The trace biomass production we detect at sub-freezing temperatures is not of sufficient magnitude to result in substantial community shifts (Figures 2 and 3) but supports previous observations of trace microbial activity at temperatures below freezing (Bakermans et al., 2003; Nikrad et al., 2016; Rivkina et al., 2000; Tuorto et al., 2014). Temperature does not appear to drive differences in growth rate, but does exert control over which taxa grow. Permafrost microbial communities host organisms with a wide range of growth temperature preferences, and the speed of this growth is likely driven by the difference between optimal growth temperature and thaw temperature, rather than temperature itself, as has been suggested through in vitro studies of permafrost isolates (Ernakovich & Wallenstein, 2015; Panikov & Sizova, 2007). This concept is supported by recent SIP studies of soil warming, which similarly support the finding that temperature affects the identity of growing taxa more than their growth rates (Metze et al., 2024).

The recalcitrance of necromass-derived DNA in the environment is of concern for the interpretation of genomic data from environmental samples. Necromass-derived DNA has been demonstrated to account for a substantial fraction of DNA recovered for microbial community analysis (Carini et al., 2016). Thus, some of the DNA extracted in this study is likely representative of relict DNA contributing to 16S results. However, previous work at the Fox Permafrost Tunnel has shown that living microbial community composition is imprinted onto the relict DNA pool. Therefore, descriptions of microbial community structure at this site are likely not substantially biased by the inclusion of relic DNA (Burkert et al., 2019). Still, during microbial community succession, subtle changes to taxonomic composition of the community may be obscured by the persistence of relict DNA. Future studies to examine biomolecular persistence are needed to interpret genomic- and SIP-based studies more faithfully in cold environments.

A limitation of this study is that microcosm incubations, even under tightly controlled analog conditions, cannot perfectly replicate the stochasticity of in situ permafrost thaw at the landscape scale. In a true thaw scenario, it is conceivable that increased hydrological connectivity would lead to increased rates of microbial dispersal. If dispersal is limited, environmental filtering may dominate the composition of the microbial community, but increased dispersal rates could lead to increased microbial community functioning due to the arrival of surface bacteria that are well-adapted to thawed conditions and potentially more capable of rapid growth—such organisms could quickly over-shadow an ancient community (Bottos et al., 2018; Ernakovich et al., 2022; Graham & Stegen, 2017). As closed systems, our incubations do not experience thaw-induced input from surface microbial communities or hydrologic communication with surrounding subsurface permafrost environments. Furthermore, hydrological intrusion could supply oxygen that, in turn, could allow more rapid degradation of recalcitrant organic matter that is difficult or impossible to degrade anaerobically (Wilmoth et al., 2021). The smaller organic moieties produced may provide a suitable substrate for fermentation and methanogenesis once introduced O_2 is consumed. Future studies of microbial growth and succession in subsurface permafrost would benefit from examining the impact of mixing, dispersal, oxygenation, and/or seeding from surface environments. Even in the absence of dispersal, our study demonstrates that resuscitated microorganisms have a remarkable capacity for growth, with the potential for dramatic reshaping of the microbial community during extended thaw conditions (Figure 3, Figures S9–S13 in Supporting Information S1).

3.6. Gas Production is Heterogenous and Difficult to Predict

Over the course of our anaerobic lipid-SIP incubations, we tracked the evolution of CO_2 and CH_4 in incubation headspace by GC-FID (Figure 5). CO_2 production was most rapid in near-surface permafrost, with a 30-day production rate of 3.1×10^{-1} nmol ml^{-1} g^{-1} day^{-1}. CH_4 emission was relatively muted in near-surface permafrost (2.1×10^{-4} nmol ml^{-1} g^{-1} day^{-1}). In contrast, CH_4 efflux was greater in subsurface samples (3.8×10^{-4} to 1×10^{-2} nmol ml^{-1} g^{-1} day^{-1}). CH_4 emission decreased with distance from the tunnel portal, but due to the similarities in permafrost age (Table 1) we are hesitant to attribute differences in methane emission to permafrost age or to microbial community composition (Figure S8 in Supporting Information S1).

CO_2 and CH_4 production observed over the course of these incubations represents not only gases produced by biological activity during the course of the SIP incubation but also biogenic gas entrained within the permafrost matrix, accumulated over millennia and/or emplaced during initial deposition (Rivkina et al., 2007), liberated by the processes of thaw or the introduction of the isotopic tracer. These sources are difficult to disentangle. Our observed heterogeneity in gas production is likely the compounding of multiple factors: quantities of trapped gas, microbial community composition, thaw temperature, and availability of organic substrates and electron donors/acceptors. In our study, production of methane does not clearly relate to the abundance of methanogenic taxa (Figure 5, Figure S8 in Supporting Information S1) nor to the incubation temperature, as one would expect if biological methanogenesis was the primary contributor during early thaw. Indeed, it is possible that biogenic methane was not produced over the course of our incubation at all and observed emissions are instead from methane entrained in the permafrost matrix. Methanogenic archaea may require substantial "priming" of their environment by bacteria (e.g., the production of H_2 or methylated fermentation products) to produce their necessary substrates regardless of anaerobic conditions (Ellenbogen et al., 2023). Previous anaerobic permafrost incubations have observed lag times of up to a year before methanogenesis is observed (Yang et al., 2021).

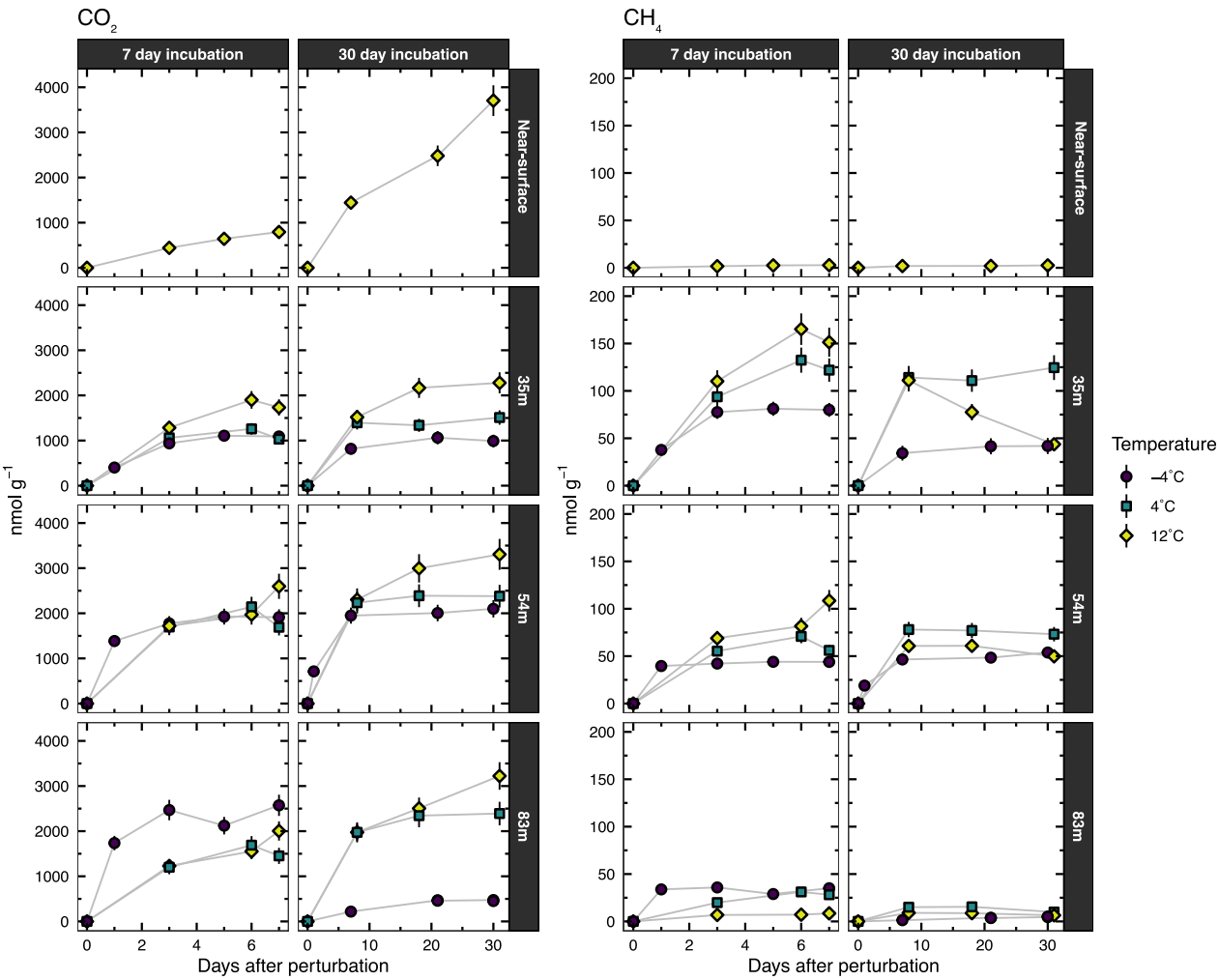

Figure 5. Carbon dioxide and methane efflux. Gas efflux is reported in nmol gas per gram of permafrost (wet weight). Error bars represent the standard error of the calibration. Note differences in horizontal axes between 7 and 30 days incubations as well as differences in vertical axes between CO_2 (left) and CH_4 (right) panels.

3.7. Areas for Future Investigation

One implication of this work is that the magnitude of ongoing warming appears less important than the lengthening of the thaw season for liberating recalcitrant C in subsurface permafrost. Even with increasing warmth and a deeper active thaw layer, as long as the warm season is short enough (i.e., refreezing takes place before the resuscitation and growth lag time) and conditions remain anaerobic (as in this study), subsurface microorganisms may not be able to resuscitate within the thaw window. GHG in the short term may therefore be dominated by [ancient] gases entrained in the frozen matrix, rather than those freshly produced. Therefore, in addition to temperature, the periodicity of the freeze/thaw interval, and the transport of O_2 into subsurface horizons, and their relation to microbial resuscitation and growth capacity, may be a critical parameter to consider for model-based predictions of biogeochemical responses to warming regions.

This study focuses on discontinuous, syngenetic near-surface and subsurface permafrost in interior Alaska. Many other kinds of permafrost exist in Alaska and elsewhere throughout cold regions. For example, continuous permafrost on Alaska's north slope and in Siberia extends hundreds of meters to over a kilometer into the subsurface (Jorgenson et al., 2008). Whether permafrost at these extreme depths will exhibit similar rates of microbial resuscitation and growth given ongoing warming remains an open question. Furthermore, the factors controlling the limits of life in deep subsurface permafrost habitability have not been thoroughly investigated. While some hyperarid soils have been described as essentially sterile, with microbial biosignatures falling below detection as

conditions grow increasingly hostile (Dragone et al., 2021), it is unknown if similar gradients can be found in deep permafrost. This begs the question: in deep subsurface permafrost, does there exist a fringe beyond which signatures of microbial activity can no longer be detected? How will these deep horizons respond to a changing climate?

4. Conclusions

In this study, we quantify microbial growth rates and resuscitation in near-surface and subsurface permafrosts under a range of thaw scenarios. Across our samples, microbial resuscitation is detected as early as 1 week following thaw disturbance. However, the degree of microbial growth and proliferation varies substantially between near-surface and subsurface sites. Subsurface permafrosts exhibit extremely low rates of biomass production after 30 days and only an estimated 0.001%–0.01% of the microbial community is resuscitated on a daily basis. The exceedingly slow resuscitation and thaw rates in early permafrost thaw, and an apparent lack of temperature dependence, indicate that thaw duration, rather than temperature, is the key control on microbial populations. Because microbial resuscitation and growth does not clearly relate to the thaw temperature, we propose that factors other than temperature—such as nutrient availability and taxonomic composition—primarily control resuscitation and biomass production. In subsurface samples, production of glycolipids is more robust than phospholipids, and the opposite is true in near-surface samples, suggesting a key physiological role for glycolipids in long term cryoprotection during burial. In all thawed conditions (incubations held above 0°C), microbial communities undergo dramatic restructuring after 6 months, often with previously trace microbial constituents becoming dominant members of the community. Finally, under the anaerobic conditions tested in this study, CO_2 is emitted more rapidly in near-surface than subsurface permafrost. Conversely, CH_4 is emitted more readily in subsurface permafrost. Taxonomic indicators of biological methanogenesis (i.e., the presence of *Methanobacterium* and other methanogenic archaea) do not clearly relate to the emission of CH_4. Overall, gas emissions from subsurface permafrost do not follow clear trends with temperature. Our study is the first to apply stable ^2H lipid stable isotope probing to permafrosts, and, to our knowledge, represents the first measurement of in situ microbial growth rates in subsurface permafrost. Future efforts deploying lipid-SIP in permafrost-hosted environments may further elucidate the timing of microbial resuscitation and growth under a wider range of environmental perturbations, and how anabolic activity maps onto ecosystem-scale carbon cycle processes and GHG emissions. This work represents an initial contribution to assessing biological activity in deep permafrost environments under warming scenarios, a task urgently required for assessing the biogeochemical implications of the ongoing warming of cold regions.

Conflict of Interest

The authors declare no conflicts of interest relevant to this study.

Data Availability Statement

Raw data generated during this study is available at https://osf.io/fm5ux/ (Caro & Jech, 2024). Processed data and data analysis scripts are available on Zenodo at https://doi.org/10.5281/zenodo.14624685 (Caro et al., 2025).

Acknowledgments
We thank Noah Fierer and Kevin Rozmiarek for valuable discussions during the preparation of this manuscript. We thank three anonymous peer-reviewers for feedback that improved the content of the manuscript. We thank Rachel Mackelprang, Joy O'Brien, Gareth Trubl, Karl Romanowicz, and Duane Froese for advice during the design of the study, and Eli Deeb for assistance with sample collection. Isotopic determination of heavy water tracer solutions was conducted by the Feng Lab at Dartmouth College, with sincere thanks to Wil Leavitt. Soil geochemistry was analyzed at the Colorado State University Soil and Water Testing Laboratory. Isotope ratio mass spectrometry was conducted at the CU Boulder Earth Systems Stable Isotope Lab (CUBES-SIL) core facility (RRID: SCR_019300). 16S amplification, cleanup, and sequencing was carried out at the University of Colorado Boulder Center for Microbial Exploration with thanks to Jessica Henley. T. Caro was supported by an NSF Graduate Research Fellowship. T. Caro and S. Jech were supported through the IQ Biology Program of the BioFrontiers Institute at the University of Colorado, Boulder. NOSAMS is supported by the NSF Cooperative Agreement number, OCE-1755125. This work was funded by a U.S. Army Research Office grant (W911NF2120119/78484-LS) awarded to S. Kopf. T. Douglas was supported by the Strategic Environmental Research and Development Program (project RC18-1170) and the Environmental Security Technology Demonstration Program (project RC22-7408). R. Barbato acknowledges funding from the US Department of Defense—PE 0602144A Program Increase "Defense Resiliency Platform Against Extreme Cold Weather".

References

Aanderud, Z. T., Jones, S. E., Fierer, N., & Lennon, J. T. (2015). Resuscitation of the rare biosphere contributes to pulses of ecosystem activity. *Frontiers in Microbiology*, *6*, 24. https://doi.org/10.3389/fmicb.2015.00024

Apprill, A., McNally, S., Parsons, R., & Weber, L. (2015). Minor revision to V4 region SSU rRNA 806R gene primer greatly increases detection of SAR11 bacterioplankton. *Aquatic Microbial Ecology*, *75*(2), 129–137. https://doi.org/10.3354/ame01753

Bakermans, C., Tsapin, A. I., Souza-Egipsy, V., Gilichinsky, D. A., & Nealson, K. H. (2003). Reproduction and metabolism at—10°C of bacteria isolated from Siberian permafrost. *Environmental Microbiology*, *5*(4), 321–326. https://doi.org/10.1046/j.1462-2920.2003.00419.x

Barbato, R. A., Jones, R. M., Douglas, T. A., Doherty, S. J., Messan, K., Foley, K., et al. (2022). Not all permafrost microbiomes are created equal: Influence of permafrost thaw on the soil microbiome in a laboratory incubation study. *Soil Biology and Biochemistry*, *167*, 108605. https://doi.org/10.1016/j.soilbio.2022.108605

Barnett, D. J. M., Arts, I. C. W., & Penders, J. (2021). microViz: An R package for microbiome data visualization and statistics. *Journal of Open Source Software*, *6*(63), 3201. https://doi.org/10.21105/joss.03201

Bligh, E. G., & Dyer, W. J. (1959). A rapid method of total lipid extraction and purification. *Canadian Journal of Biochemistry and Physiology*, *37*(8), 911–917. https://doi.org/10.1139/o59-099

Bottos, E. M., Kennedy, D. W., Romero, E. B., Fansler, S. J., Brown, J. M., Bramer, L. M., et al. (2018). Dispersal limitation and thermodynamic constraints govern spatial structure of permafrost microbial communities. *FEMS Microbiology Ecology*, *94*(8), fiy110. https://doi.org/10.1093/femsec/fiy110

Boutard, M., Cerisy, T., Nogue, P.-Y., Alberti, A., Weissenbach, J., Salanoubat, M., & Tolonen, A. C. (2014). Functional diversity of carbohydrate-active enzymes enabling a bacterium to ferment plant biomass. *PLoS Genetics*, *10*(11), e1004773. https://doi.org/10.1371/journal.pgen.1004773

Buehler, A. J., Martin, N. H., Boor, K. J., & Wiedmann, M. (2018). Psychrotolerant spore-former growth characterization for the development of a dairy spoilage predictive model. *Journal of Dairy Science*, *101*(8), 6964–6981. https://doi.org/10.3168/jds.2018-14501

Burkert, A., Douglas, T. A., Waldrop, M. P., & Mackelprang, R. (2019). Changes in the active, dead, and dormant microbial community structure across a Pleistocene permafrost chronosequence. *Applied and Environmental Microbiology*, *85*(7), e02646-18. https://doi.org/10.1128/aem.02646-18

Callahan, B. J., McMurdie, P. J., Rosen, M. J., Han, A. W., Johnson, A. J. A., & Holmes, S. P. (2016). DADA2: High-resolution sample inference from Illumina amplicon data. *Nature Methods*, *13*(7), 581–583. https://doi.org/10.1038/nmeth.3869

Carini, P., Marsden, P. J., Leff, J. W., Morgan, E. E., Strickland, M. S., & Fierer, N. (2016). Relic DNA is abundant in soil and obscures estimates of soil microbial diversity. *Nature Microbiology*, *2*(3), 1–6. https://doi.org/10.1038/nmicrobiol.2016.242

Caro, T., & Jech, S. (2024). Permafrost lipid-SIP [Dataset]. *Open Science Framework*. https://osf.io/fm5ux/

Caro, T., Kopf, S., & Jech, S. (2025). tacaro/permafrost_LHSIP: v1.0 [Software]. *Zenodo*. https://doi.org/10.5281/zenodo.14624684

Caro, T. A., Kashyap, S., Brown, G., Chen, C., Kopf, S. H., & Templeton, A. S. (2024). Single-cell measurement of microbial growth rate with Raman microspectroscopy. *FEMS Microbiology Ecology*, *100*(9), fiae110. https://doi.org/10.1093/femsec/fiae110

Caro, T. A., McFarlin, J., Jech, S., Fierer, N., & Kopf, S. (2023). Hydrogen stable isotope probing of lipids demonstrates slow rates of microbial growth in soil. *Proceedings of the national academy of sciences* (Vol. 120(16), p. e2211625120). https://doi.org/10.1073/pnas.2211625120

Casillo, A., Parrilli, E., Tutino, M. L., & Corsaro, M. M. (2019). The outer membrane glycolipids of bacteria from cold environments: Isolation, characterization, and biological activity. *FEMS Microbiology Ecology*, *95*(7), fiz094. https://doi.org/10.1093/femsec/fiz094

Chades, T., Scully, S. M., Ingvadottir, E. M., & Orlygsson, J. (2018). Fermentation of mannitol extracts from brown macro algae by thermophilic Clostridia. *Frontiers in Microbiology*, *9*, 1931. https://doi.org/10.3389/fmicb.2018.01931

Corsaro, M. M., Casillo, A., Parrilli, E., & Tutino, M. L. (2017). Molecular structure of lipopolysaccharides of cold-adapted bacteria. In R. Margesin (Ed.), *Psychrophiles: From biodiversity to biotechnology* (pp. 285–303). Springer International Publishing.

Doherty, S. J., Barbato, R. A., Grandy, A. S., Thomas, W. K., Monteux, S., Dorrepaal, E., et al. (2020). The transition from stochastic to deterministic bacterial community assembly during permafrost thaw succession. *Frontiers in Microbiology*, *11*, 596589. https://doi.org/10.3389/fmicb.2020.596589

Douglas, T. A., Fortier, D., Shur, Y. L., Kanevskiy, M. Z., Guo, L., Cai, Y., & Bray, M. T. (2011). Biogeochemical and geocryological characteristics of wedge and thermokarst-cave ice in the CRREL permafrost tunnel, Alaska. *Permafrost and Periglacial Processes*, *22*(2), 120–128. https://doi.org/10.1002/ppp.709

Dragone, N. B., Diaz, M. A., Hogg, I. D., Lyons, W. B., Jackson, W. A., Wall, D. H., et al. (2021). Exploring the boundaries of microbial habitability in soil. *Journal of Geophysical Research: Biogeosciences*, *126*(6), e2020JG006052. https://doi.org/10.1029/2020jg006052

Eichorst, S. A., Strasser, F., Woyke, T., Schintlmeister, A., Wagner, M., & Woebken, D. (2015). Advancements in the application of NanoSIMS and Raman microspectroscopy to investigate the activity of microbial cells in soils. *FEMS Microbiology Ecology*, *91*(10), fiv106. https://doi.org/10.1093/femsec/fiv106

Ellenbogen, J. B., Borton, M. A., McGivern, B. B., Cronin, D. R., Hoyt, D. W., Freire-Zapata, V., et al. (2023). Methylotrophy in the Mire: Direct and indirect routes for methane production in thawing permafrost. *MSystems*, *9*(1), e00698-23. https://doi.org/10.1128/msystems.00698-23

Epstein, S. S. (2009). Microbial awakenings. *Nature*, *457*(7233), 1083-1083. https://doi.org/10.1038/4571083a

Ernakovich, J. G., Barbato, R. A., Rich, V. I., Schädel, C., Hewitt, R. E., Doherty, S. J., et al. (2022). Microbiome assembly in thawing permafrost and its feedbacks to climate. *Global Change Biology*, *28*(17), 5007–5026. https://doi.org/10.1111/gcb.16231

Ernakovich, J. G., & Wallenstein, M. D. (2015). Permafrost microbial community traits and functional diversity indicate low activity at in situ thaw temperatures. *Soil Biology and Biochemistry*, *87*, 78–89. https://doi.org/10.1016/j.soilbio.2015.04.009

Evans, P. N., Parks, D. H., Chadwick, G. L., Robbins, S. J., Orphan, V. J., Golding, S. D., & Tyson, G. W. (2015). Methane metabolism in the archaeal phylum Bathyarchaeota revealed by genome-centric metagenomics. *Science*, *350*(6259), 434–438. https://doi.org/10.1126/science.aac7745

Foley, M. M., Stone, B. W. G., Caro, T. A., Sokol, N. W., Koch, B. J., Blazewicz, S. J., et al. (2024). Growth rate as a link between microbial diversity and soil biogeochemistry. *Nature Ecology and Evolution*, *8*(11), 1–9. https://doi.org/10.1038/s41559-024-02520-7

Frostegård, A., & Bååth, E. (1996). The use of phospholipid fatty acid analysis to estimate bacterial and fungal biomass in soil. *Biology and Fertility of Soils*, *22*(1), 59–65. https://doi.org/10.1007/s003740050076

Frostegård, Å., Tunlid, A., & Bååth, E. (2011). Use and misuse of PLFA measurements in soils. *Soil Biology and Biochemistry*, *43*(8), 1621–1625. https://doi.org/10.1016/j.soilbio.2010.11.021

Gilichinsky, D. A., Soina, V. S., & Petrova, M. A. (1993). Cryoprotective properties of water in the Earth cryolithosphere and its role in exobiology. *Origins of Life and Evolution of the Biosphere*, *23*(1), 65–75. https://doi.org/10.1007/bf01581991

Graham, E. B., & Stegen, J. C. (2017). Dispersal-based microbial community assembly decreases biogeochemical function. *Processes*, *5*(4), 65. https://doi.org/10.3390/pr5040065

Griffiths, M. J., van Hille, R. P., & Harrison, S. T. L. (2010). Selection of direct transesterification as the preferred method for assay of fatty acid content of microalgae. *Lipids*, *45*(11), 1053–1060. https://doi.org/10.1007/s11745-010-3468-2

Guan, Z., & Goldfine, H. (2021). Lipid diversity in Clostridia. *Biochimica et Biophysica Acta (BBA): Molecular and Cell Biology of Lipids*, *1866*(9), 158966. https://doi.org/10.1016/j.bbalip.2021.158966

He, Y., Li, M., Perumal, V., Feng, X., Fang, J., Xie, J., et al. (2016). Genomic and enzymatic evidence for acetogenesis among multiple lineages of the archaeal phylum bathyarchaeota widespread in marine sediments. *Nature Microbiology*, *1*(6), 1–9. https://doi.org/10.1038/nmicrobiol.2016.35

Hippe, H., & Stackebrandt, E. (2015). Desulfosporosinus. In *Bergey's manual of systematics of archaea and bacteria* (pp. 1–10). John Wiley and Sons, Ltd.

Hugelius, G., Strauss, J., Zubrzycki, S., Harden, J. W., Schuur, E. a. G., Ping, C. L., et al. (2014). Estimated stocks of circumpolar permafrost carbon with quantified uncertainty ranges and identified data gaps. *Biogeosciences*, *11*(23), 6573–6593. https://doi.org/10.5194/bg-11-6573-2014

Jones, R. A., Shropshire, H., Zhao, C., Murphy, A., Lidbury, I., Wei, T., et al. (2021). Phosphorus stress induces the synthesis of novel glycolipids in Pseudomonas aeruginosa that confer protection against a last-resort antibiotic. *The ISME Journal*, *15*(11), 3303–3314. https://doi.org/10.1038/s41396-021-01008-7

Jorgenson, M., Yoshikawa, K., Kanevskiy, M., Shur, Y., Romanovsky, V., et al. (2008). Permafrost characteristics of Alaska + Map.

Kopf, S., Davidheiser-Kroll, B., & Kocken, I. (2021). Isoreader: An R package to read stable isotope data files for reproducible research. *Journal of Open Source Software*, *6*(61), 2878. https://doi.org/10.21105/joss.02878

Kopf, S. H., McGlynn, S. E., Green-Saxena, A., Guan, Y., Newman, D. K., & Orphan, V. J. (2015). Heavy water and 15N labelling with NanoSIMS analysis reveals growth rate-dependent metabolic heterogeneity in chemostats. *Environmental Microbiology*, *17*(7), 2542–2556. https://doi.org/10.1111/1462-2920.12752

Kopf, S. H., Sessions, A. L., Cowley, E. S., Reyes, C., Van Sambeek, L., Hu, Y., et al. (2016). Trace incorporation of heavy water reveals slow and heterogeneous pathogen growth rates in cystic fibrosis sputum. *Proceedings of the National Academy of Sciences* (Vol. 113(2), pp. E110–E116). https://doi.org/10.1073/pnas.1512057112

Krishnamurthi, S., Ruckmani, A., Pukall, R., & Chakrabarti, T. (2010). *Psychrobacillus* gen. Nov. and proposal for reclassification of *Bacillus insolitus* Larkin & Stokes, 1967, *B. psychrotolerans* Abd-El Rahman et al., 2002 and *B. psychrodurans* Abd-El Rahman et al., 2002 as *Psychrobacillus insolitus* comb. Nov., *Psychrobacillus psychrotolerans* comb. Nov. and *Psychrobacillus psychrodurans* comb. Nov. *Systematic & Applied Microbiology*, *33*(7), 367–373. https://doi.org/10.1016/j.syapm.2010.06.003

Lazar, C. S., Baker, B. J., Seitz, K., Hyde, A. S., Dick, G. J., Hinrichs, K., & Teske, A. P. (2016). Genomic evidence for distinct carbon substrate preferences and ecological niches of bathyarchaeota in estuarine sediments. *Environmental Microbiology*, *18*(4), 1200–1211. https://doi.org/10.1111/1462-2920.13142

Leewis, M.-C., Berlemont, R., Podgorski, D. C., Srinivas, A., Zito, P., Spencer, R. G. M., et al. (2020). Life at the frozen limit: Microbial carbon metabolism across a late Pleistocene permafrost chronosequence. *Frontiers in Microbiology*, *11*, 1753. https://doi.org/10.3389/fmicb.2020.01753

Lennon, J. T., & Jones, S. E. (2011). Microbial seed banks: The ecological and evolutionary implications of dormancy. *Nature Reviews Microbiology*, *9*(2), 119–130. https://doi.org/10.1038/nrmicro2504

Lipp, J. S., Morono, Y., Inagaki, F., & Hinrichs, K.-U. (2008). Significant contribution of Archaea to extant biomass in marine subsurface sediments. *Nature*, *454*(7207), 991–994. https://doi.org/10.1038/nature07174

Mackelprang, R., Burkert, A., Haw, M., Mahendrarajah, T., Conaway, C. H., Douglas, T. A., & Waldrop, M. P. (2017). Microbial survival strategies in ancient permafrost: Insights from metagenomics. *The ISME Journal*, *11*(10), 2305–2318. https://doi.org/10.1038/ismej.2017.93

McMurdie, P. J., & Holmes, S. (2013). Phyloseq: An R package for reproducible interactive analysis and graphics of microbiome census data. *PLoS One*, *8*(4), e61217. https://doi.org/10.1371/journal.pone.0061217

Meija, J., Coplen, T. B., Berglund, M., Brand, W. A., Bièvre, P. D., Gröning, M., et al. (2016). Isotopic compositions of the elements 2013 (IUPAC Technical Report). *Pure and Applied Chemistry*, *88*(3), 293–306. https://doi.org/10.1515/pac-2015-0503

Metze, D., Schnecker, J., de Carlan, C. L. N., Bhattarai, B., Verbruggen, E., Ostonen, I., et al. (2024). Soil warming increases the number of growing bacterial taxa but not their growth rates. *Science Advances*, *10*(8), eadk6295. https://doi.org/10.1126/sciadv.adk6295

Mu, C., Zhang, T., Wu, Q., Cao, B., Zhang, X., Peng, X., et al. (2015). Carbon and nitrogen properties of permafrost over the Eboling Mountain in the upper reach of Heihe River Basin, Northwestern China. *Arctic Antarctic and Alpine Research*, *47*(2), 203–211. https://doi.org/10.1657/aaar00c-13-095

Nikrad, M. P., Kerkhof, L. J., & Häggblom, M. M. (2016). The subzero microbiome: Microbial activity in frozen and thawing soils. *FEMS Microbiology Ecology*, *92*(6), fiw081. https://doi.org/10.1093/femsec/fiw081

Panikov, N. S., & Sizova, M. V. (2007). Growth kinetics of microorganisms isolated from Alaskan soil and permafrost in solid media frozen Down to −35°C. *FEMS Microbiology Ecology*, *59*(2), 500–512. https://doi.org/10.1111/j.1574-6941.2006.00210.x

Parada, A. E., Needham, D. M., & Fuhrman, J. A. (2016). Every base matters: Assessing small subunit rRNA primers for marine microbiomes with mock communities, time series and global field samples. *Environmental Microbiology*, *18*(5), 1403–1414. https://doi.org/10.1111/1462-2920.13023

Peng, Z., Feng, L., Wang, X., & Miao, X. (2019). Adaptation of synechococcus sp. PCC 7942 to phosphate starvation by glycolipid accumulation and membrane lipid remodeling. *Biochimica et Biophysica Acta (BBA): Molecular and Cell Biology of Lipids*, *1864*(12), 158522. https://doi.org/10.1016/j.bbalip.2019.158522

Price, P. B., & Sowers, T. (2004). Temperature dependence of metabolic rates for microbial growth, maintenance, and survival. *Proceedings of the National Academy of Sciences* (Vol. 101(13), pp. 4631–4636). https://doi.org/10.1073/pnas.0400522101

Putman, A. L., Feng, X., Sonder, L. J., & Posmentier, E. S. (2017). Annual variation in event-scale precipitation δ^2H at barrow, AK, reflects vapor source region. *Atmospheric Chemistry and Physics*, *17*(7), 4627–4639. https://doi.org/10.5194/acp-17-4627-2017

Quast, C., Pruesse, E., Yilmaz, P., Gerken, J., Schweer, T., Yarza, P., et al. (2013). The SILVA ribosomal RNA gene database project: Improved data processing and web-based tools. *Nucleic Acids Research*, *41*(D1), D590–D596. https://doi.org/10.1093/nar/gks1219

Quideau, S. A., McIntosh, A. C. S., Norris, C. E., Lloret, E., Swallow, M. J. B., & Hannam, K. (2016). Extraction and analysis of microbial phospholipid fatty acids in soils. *Journal of Visualized Experiments: JoVE*(114), 54360. https://doi.org/10.3791/54360

Rantanen, M., Karpechko, A. Y., Lipponen, A., Nordling, K., Hyvärinen, O., Ruosteenoja, K., et al. (2022). The Arctic has warmed nearly four times faster than the globe since 1979. *Communications Earth & Environment*, *3*(1), 1–10. https://doi.org/10.1038/s43247-022-00498-3

Rivkina, E., Shcherbakova, V., Laurinavichius, K., Petrovskaya, L., Krivushin, K., Kraev, G., et al. (2007). Biogeochemistry of methane and methanogenic archaea in permafrost. *FEMS Microbiology Ecology*, *61*(1), 1–15. https://doi.org/10.1111/j.1574-6941.2007.00315.x

Rivkina, E. M., Friedmann, E. I., McKay, C. P., & Gilichinsky, D. A. (2000). Metabolic activity of permafrost bacteria below the freezing point. *Applied and Environmental Microbiology*, *66*(8), 3230–3233. https://doi.org/10.1128/aem.66.8.3230-3233.2000

Rodríguez-Ruiz, J., Belarbi, E.-H., Sánchez, J. L. G., & Alonso, D. L. (1998). Rapid simultaneous lipid extraction and transesterification for fatty acid analyses. *Biotechnology Techniques*, *12*(9), 689–691. https://doi.org/10.1023/a:1008812904017

Romanowicz, K. J., & Kling, G. W. (2022). Summer thaw duration is a strong predictor of the soil microbiome and its response to permafrost thaw in arctic tundra. *Environmental Microbiology*, *24*(12), 6220–6237. https://doi.org/10.1111/1462-2920.16218

Schubotz, F., Wakeham, S. G., Lipp, J. S., Fredricks, H. F., & Hinrichs, K.-U. (2009). Detection of microbial biomass by intact polar membrane lipid analysis in the water column and surface sediments of the Black Sea. *Environmental Microbiology*, *11*(10), 2720–2734. https://doi.org/10.1111/j.1462-2920.2009.01999.x

Spring, S., Merkhoffer, B., Weiss, N., Kroppenstedt, R. M., Hippe, H., & Stackebrandt, E. (2003). Characterization of novel psychrophilic clostridia from an Antarctic microbial mat: Description of Clostridium frigoris sp. Nov., Clostridium lacusfryxellense sp. Nov., Clostridium bowmanii sp. Nov. and Clostridium psychrophilum sp. Nov. and reclassification of Clostridium laramiense as Clostridium estertheticum subsp. laramiense subsp. Nov. *International Journal of Systematic and Evolutionary Microbiology*, *53*(4), 1019–1029. https://doi.org/10.1099/ijs.0.02554-0

Stankeviciute, G., Guan, Z., Goldfine, H., & Klein, E. A. (2019). Caulobacter crescentus adapts to phosphate starvation by synthesizing anionic glycoglycerolipids and a novel glycosphingolipid. *MBio*, *10*(2), e00107-19. https://doi.org/10.1128/mbio.00107-19

Stocker, T. (2014). *Climate change 2013: The physical science basis: Working group I contribution to the fifth assessment report of the intergovernmental panel on climate change*. Cambridge University Press.

Tuorto, S. J., Darias, P., McGuinness, L. R., Panikov, N., Zhang, T., Häggblom, M. M., & Kerkhof, L. J. (2014). Bacterial genome replication at subzero temperatures in permafrost. *The ISME Journal*, *8*(1), 139–149. https://doi.org/10.1038/ismej.2013.140

Waldrop, M. P., Chabot, C. L., Liebner, S., Holm, S., Snyder, M. W., Dillon, M., et al. (2023). Permafrost microbial communities and functional genes are structured by latitudinal and soil geochemical gradients. *ISME Journal*, *17*(8), 1–12. https://doi.org/10.1038/s41396-023-01429-6

Wegener, G., Bausch, M., Holler, T., Thang, N. M., Prieto, M. X., Kellermann, M. Y., et al. (2012). Assessing sub-seafloor microbial activity by combined stable isotope probing with deuterated water and 13C-bicarbonate. *Environmental Microbiology*, *14*(6), 1517–1527. https://doi.org/10.1111/j.1462-2920.2012.02739.x

Weissman, J. L., Hou, S., & Fuhrman, J. A. (2021). Estimating maximal microbial growth rates from cultures, metagenomes, and single cells via codon usage patterns. *PNAS*, *118*(12), e2016810118. https://doi.org/10.1073/pnas.2016810118

Willers, C., Jansen van Rensburg, P. j., & Claassens, S. (2015a). Phospholipid fatty acid profiling of microbial communities–A review of interpretations and recent applications. *Journal of Applied Microbiology*, *119*(5), 1207–1218. https://doi.org/10.1111/jam.12902

Willers, C., Jansen van Rensburg, P. j., & Claassens, S. (2015b). Microbial signature lipid biomarker analysis: An approach that is still preferred, Even amid various method modifications. *Journal of Applied Microbiology*, *118*(6), 1251–1263. https://doi.org/10.1111/jam.12798

Wilmoth, J. L., Schaefer, J. K., Schlesinger, D. R., Roth, S. W., Hatcher, P. G., Shoemaker, J. K., & Zhang, X. (2021). The role of oxygen in stimulating methane production in wetlands. *Global Change Biology*, *27*(22), 5831–5847. https://doi.org/10.1111/gcb.15831

Yang, S., Liebner, S., Walz, J., Knoblauch, C., Bornemann, T. L. V., Probst, A. J., et al. (2021). Effects of a long-term anoxic warming scenario on microbial community structure and functional potential of permafrost-affected soil. *Permafrost and Periglacial Processes*, *32*(4), 641–656. https://doi.org/10.1002/ppp.2131

Zhang, Y., Zheng, N., Wang, J., Yao, H., Qiu, Q., & Chapman, S. J. (2019). High turnover rate of free phospholipids in soil confirms the classic hypothesis of PLFA methodology. *Soil Biology and Biochemistry*, *135*, 323–330. https://doi.org/10.1016/j.soilbio.2019.05.023